Atmos. Meas. Tech., 9, 3987–3998, 2016
www.atmos-meas-tech.net/9/3987/2016/
doi:10.5194/amt-9-3987-2016


Atmospheric Measurement Techniques
Open Access
EGU

# A wavelength-dispersive instrument for characterizing fluorescence and scattering spectra of individual aerosol particles on a substrate

**Donald R. Huffman**[1], **Benjamin E. Swanson**[2], **and J. Alex Huffman**[2]

[1]University of Arizona, Department of Physics, Tucson, Arizona, USA
[2]University of Denver, Department of Chemistry and Biochemistry, Denver, Colorado, USA

*Correspondence to:* J. Alex Huffman (alex.huffman@du.edu)

Received: 3 May 2016 – Published in Atmos. Meas. Tech. Discuss.: 31 May 2016
Revised: 29 July 2016 – Accepted: 3 August 2016 – Published: 23 August 2016

**Abstract.** We describe a novel, low-cost instrument to acquire both elastic and inelastic (fluorescent) scattering spectra from individual supermicron-size particles in a multiparticle collection on a microscope slide. The principle of the device is based on a slitless spectroscope that is often employed in astronomy to determine the spectra of individual stars in a star cluster but had not been applied to atmospheric particles. Under excitation, most commonly by either a 405 nm diode laser or a UV light-emitting diode (LED), fluorescence emission spectra of many individual particles can be determined simultaneously. The instrument can also acquire elastic scattering spectra from particles illuminated by a white-light source. The technique also provides the ability to detect and rapidly estimate the number fraction of fluorescent particles that could contaminate a collection of non-fluorescent material, even without analyzing full spectra. Advantages and disadvantages of using black-and-white cameras compared to color cameras are given. The primary motivation for this work has been to develop an inexpensive technique to characterize fluorescent biological aerosol particles, especially particles such as pollen and mold spores that can cause allergies. An example of an iPhone-enabled device is also shown as a means for collecting data on biological aerosols at lower cost or by utilizing citizen scientists for expanded data collection.

## 1 Introduction

Primary biological aerosol particles (PBAP) suspended in the atmosphere, often termed bioaerosols, are comprised of a complex mixture of biological organisms and materials – including bacteria, fungal spores, pollen, and their fragments – and excretions of plants, animals, and microorganisms (Després et al., 2012; Fröhlich-Nowoisky et al., 2016). PBAP can influence human, animal, and agricultural health by causing disease and triggering allergies, and can influence Earth systems, such as cloud formation and the hydrological cycle, by acting as nuclei for the formation of liquid water or ice cloud droplets (Douwes et al., 2003; Möhler et al., 2007; Morris et al., 2014; Pöschl et al., 2010; Pöschl and Shiraiwa, 2015). Yet large holes in the collective understanding about atmospheric bioaerosols remain, and PBAP have become increasingly important in recent years in aerosol science due to synergistic advancements in detection technologies and in the understanding of roles these aerosols may play in the atmospheric system.

One common method for the discrimination of biological particles from the rest of atmospheric particulate matter is the use of single-particle laser-induced fluorescence (LIF). Many research groups have utilized LIF for real-time investigation of bioaerosols, often for the purpose of detecting possible agents of bioterrorism (e.g., Kiselev et al., 2011; Manninen et al., 2008; Pan et al., 2003, 2010; Saari et al., 2014; Sivaprakasam et al., 2004, 2009; Sodeau and O'Connor, 2016). Over the last 10–15 years a number of LIF instruments have also become commercially available, and they are becoming more widely used for atmospheric research. Two of the bioaerosol-LIF instruments most commonly used within the atmospheric research community are the Ultraviolet Aerodynamic Particle Sizer (UV-APS; TSI, Inc., Shoreview, MN) (Hairston et al., 1997; Huffman et al., 2010) and the Wideband Integrated Bioaerosol Sensor (WIBS; DMT, Inc., Boulder, CO) (Foot et al., 2008; Gabey et al., 2010;

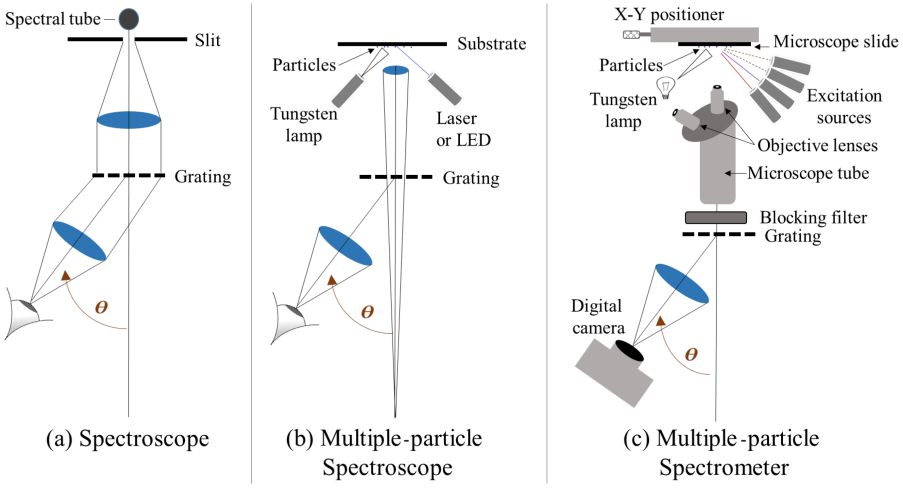


**Figure 1.** Three-stage progression of spectrometer. **(a)** Spectroscope, as often utilized in student laboratories. **(b)** Multiple-particle spectroscope. **(c)** Multiple-particle spectrometer (introduced here). For standard benchtop setup approximate distances are as follows: objective lens to grating – 20.5 cm; grating to camera – 11.4 cm.

Kaye et al., 2005; Perring et al., 2015). Both instruments allow characterization of particles with high time and size resolution but offer little spectral discrimination. The UV-APS provides aerodynamic particle-size-resolved information about ensembles of particles averaged for several seconds or minutes, and fluorescence excited at 355 nm is provided as the sample-average emission intensity in one wavelength band between 420 and 575 nm (Hairston et al., 1997). The WIBS provides optical particle size and fluorescence information for each particle interrogated, using two excitation wavelengths of 280 and 370 nm, and detects fluorescence emission in two channels for each excitation (Foot et al., 2008). Further, both instruments are quite expensive, selling for ca. USD 100 000 or more. The poor spectral resolution limits the ability of these instruments to finely discriminate between particle types, and the high cost of these instruments prevents their widespread global application.

If instruments of considerably less cost and smaller size could be developed and distributed with the capability to discriminate biological particles from non-biological material, information on the global properties of biological aerosol particles and their effect on human health and climate could be collected on a much more comprehensive scale. We have developed a low-cost instrument capable of characterizing fluorescence and white-light spectra from many individual particles collected onto a substrate, each excited at several excitation wavelengths. Here we introduce both a benchtop and a portable, smartphone-based instrument that each may serve as a transformative tool for bioaerosol detection with application to atmospheric research, pollen monitoring, and mold spore detection, among many other applications. The instrument design also has potential application to any scientific or medical diagnostic problem where a minority of approximately supermicron-sized particles can be discriminated from a majority of particles based on their fluorescence or elastic scattering spectra.

## 2 Instrument description

The instrument is built around a conventional compound microscope and uses standard glass microscope slides as particle substrates, though any non-fluorescent and relatively non-reflective material may be utilized. We will explain the principle and the details with reference to a three-stage progression of the idea as shown in Fig. 1. The optical principle is derived from the simple spectroscope as shown in Fig. 1a. In this venerable instrument, the light to be spectrally analyzed is directed onto a narrow incident slit. The light from this slit is made parallel by the collimating lens and impinges on a wavelength-dispersive element such as a prism or a transmission grating (as shown). Parallel light from the grating is dispersed into an angle $\theta$ (rad) by the grating according to the grating equation for normal incidence (Jenkins and White, 1957):

$$d \sin\theta = n\lambda, \quad (1)$$

where $d$ is the distance between rulings on the grating, $n$ is an integer giving the order of diffraction, and $\lambda$ is the wavelength of the light. For the example in Fig. 1a an atomic emission source such as H, He, or Hg is shown as the light source, which illuminates a narrow slit from behind. An image of the slit at each wavelength is dispersed according to the angle defined in Eq. (1). Because there are multiple wavelengths emitted in the visible region by the sources just mentioned, there will be a real image of the slit, which gives rise to the "line spectrum" that can be viewed with an eyepiece. This

real image can also be captured on photographic film or on an array detector such as a charge-coupled device (CCD) or complementary metal-oxide semiconductor (CMOS) detector in a digital camera.

The essential innovation of the present instrument is understood by imagining the replacement of the back-illuminated slit by one or more particles in place of the slit, held on the plane of a microscope slide as in Fig. 1b. For detection at a $\theta$ angle of zero (viewing straight through), the dark-field image appears simply as a collection of illuminated particles, and no spectral information is gained. Viewed at an appropriate angle through the transmission grating, however, the individual particles will exhibit spectral dispersion. For monochromatic illumination of a given particle, such as by a single spectral line or a laser beam, the first-order diffraction will be a single spot imaged in the same plane on which the slit image was shown previously. In the version shown in Fig. 1b, however, the image at the detector will be located at vertical and horizontal coordinates corresponding to an image of the particle's position on the substrate. For white-light illumination the dispersed image of each particle will be a swath of light with a height corresponding to the diameter of the particle and a length corresponding to the difference in dispersion angle between the limits of visible wavelengths. For example, if a particle is large in the vertical ($y$) dimension, the height of its spectral swath will be approximately equal to the vertical dimension of the particle itself. Each particle will display a rainbow of colors when viewed by eye through an eyepiece. If the substrate consists of a number of particles distributed sparsely on the surface of a microscope slide as shown in Fig. 1b, each particle will be imaged as a single, colored point for illumination by a monochromatic source; a series of different colored points for a multiple-line-emission source; or a continuum spectrum for white-light illumination.

The main idea here is the replacement of an entrance slit, which is present in most spectroscopes and the spectrographs, monochromators, and spectrometers built upon the spectroscope idea of Fig. 1a, with individual small particles, each of which effectively act as very small (two-dimensional) slits as in Fig. 1b. Thus, this instrument falls into the category of a slitless spectrometer, which has been used widely, albeit mostly in astronomical studies. In the 1880s Edward Pickering implemented the idea by placing a large prism in front of the objective lens of a refracting telescope and recording the spectral swaths on photographic film for analysis (Hale and Wadsworth, 1896). In his classic textbook George Abell (1969) has shown images of the color spectra from all stars in the famous Pleiades star cluster in one image. With this as inspiration, we produced the spectral streaks from microscopic particles that look very much like the streaks from stars through a telescope.

The incarnation of the instrument described here is relatively simple, yet it has not been applied for aerosol particle research. Other commonly applied techniques provide aspects of the benefits described here but are still distinctly different (Lakowicz, 2010). Fluorescence microscopy is widely applied in many scientific fields, but most commercial fluorescence microscopes provide fluorescence information by utilizing relatively broad-wavelength filters for excitation and emission. As a result, micrographs can be achieved that utilize a given pair of excitation and emission windows, but spectral information can only be attained by using a large sequence of filters. Laser-scanning confocal microscopy allows the user to excite a given spot with a chosen laser source and then measure the spectral dependence of the fluorescent emission, but scanning a collection of particles can be time-consuming, because the laser must raster-scan through the entire field of view, and the instrumentation is costly and relatively complicated. Fluorescence spectroscopy is achieved in the bulk phase, most often for solutions and suspensions, but is also possible for powders and solid materials, by measuring fluorescence emission spectra as the excitation wavelength is varied. In this case, highly resolved fluorescence emission spectra can be acquired, though fine spatial resolution is typically not possible, and thus the technique typically cannot provide single-particle spectra. Single-particle fluorescence instruments, such as are used for detection of atmospheric bioaerosols, normally provide very poor spectral resolution (total of one to three emission channels) and are very expensive (Foot et al., 2008; Hairston et al., 1997; Manninen et al., 2008; Sivaprakasam et al., 2004). A notable exception to the statement about spectral resolution is the single-particle fluorescence spectrometer (SPFS) developed by the Army Research Laboratory (Pan et al., 2011, 2010). This instrument can provide highly resolved spectra of individual aerosol particles suspended in air flowing through the device; however, the instrument is one-of-a-kind and is very expensive ($\gg$ USD 100 000). Thus, the instrument described here combines benefits of each of these other instrument concepts by delivering spectra of each particle in a collection on a substrate, each at a number of excitation wavelengths, and at a cost orders of magnitude lower than other techniques. Recently a similar concept of slitless microscope spectroscopy was used with silver nanoprobes applied to in vivo monitoring (Cheng et al., 2010; Xiong et al., 2013). This appears to have been the first application of slitless spectroscopy to single particles; however, the application was directed towards biomedical testing with no application to atmospheric aerosols and not towards a portable device.

### 2.1 Typical operation

Figure 1c adds some practical details about the instrument described here, the original of which was constructed from a student microscope (Model 656/98, SWIFT Microscopy, Carlsbad, CA) formerly used in an undergraduate biology teaching lab. The original vertical microscope was placed in a horizontal orientation, with the sample slide illuminated by one of several light sources consisting of diode lasers, LEDs,

or a tungsten filament light bulb. Illumination of the particles from above and to the side of the stage produces a bright particle image on a dark background – one example of so-called dark field illumination. The microscope stage with its attached $x$–$y$ positioner and the objective lens turret were retained from the original microscope. The eyepiece, or ocular lens, was removed and placed on a rail that rotates about a pivot point located in the plane of the transmission diffraction grating (300 grooves $mm^{-1}$; Thor Labs, Inc., GT25-03). A standard optical table with mounting holes spaced on a 1 in. grid supports optical rails and holders secured to it for mounting the optical components (Thor Labs, Inc.). Various cameras, both color and black and white (b/w), have been adapted with mounts to the rotating detector arm. See Table S1 in the Supplement for details regarding specifications of cameras discussed here.

In operation, when the camera arm is set at 0°, the instrument operates as a standard microscope. At the approximate angle of first-order diffraction (e.g., ca. 11° for red, 7° for blue light as defined by Eq. 1) the camera will record spectral swaths of each particle in the field of view. We note that either elastic scattering (no change in wavelength upon scattering) or inelastic scattering (change of wavelength upon scattering) can be recorded. In all cases discussed in this paper inelastic scattering is due to fluorescence, though the concept should apply to inelastic Raman scattering, for example, and this will be investigated in future research. Thus the instrument has the capability of recording either elastic or inelastic scattering from individual particles in its field of view (on the order of 1.0 mm wide by 0.7 mm high under 10× magnification), depending on the type of particle and the illumination source. An additional optical element necessary for fluorescence spectroscopy is a long-pass blocking filter which we place between the objective lens and the grating. The filter is selected to block the transmission of monochromatic light from the excitation source, while allowing transmission of as much of the fluorescence spectrum as possible. For example, we commonly use a diode laser with a wavelength of about 405 nm and long-pass filters chosen to block wavelengths below ca. 420 or 440 nm (Edmund Optics, 832916-10). We have also used 280, 350, 370, and 450 nm excitation sources, but the process and concept remain the same.

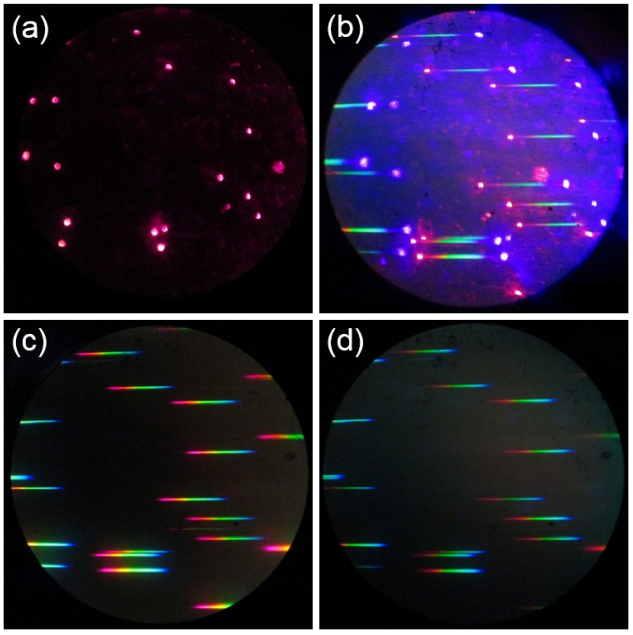


**Figure 2.** Four-panel progression of images acquired for a given scene of paper mulberry pollen particles collected onto a glass microscope slide, analyzed using 10× objective. Scale is the same in each figure, with each horizontal swath of color approximately 10 µm in height. **(a)** Dark field image of particles illuminated by monochromatic red laser light ($\theta = 0$). **(b)** Particles illuminated with both violet (405 nm) and red (650 nm) diode lasers. Fluorescence spectra of individual particles showing image taken without use of blocking filter. **(c)** White-light illumination with tungsten filament bulb. **(d)** Fluorescence emission with excitation from violet diode laser, but using blocking filter to remove violet laser point. Canon Powershot A2300 HD camera utilized offers 4608 × 3456 square pixels 1.3 µm in size.

## 2.2 Example spectra and data analysis

Individual panels of Fig. 2 (a through d) serve to illustrate the different types of images collected during standard operation. All panels of Fig. 2 show the same sample of paper mulberry pollen (*Broussonetia papyrifera*; 12–13 µm; Thermo Fisher Scientific) as an example, collected onto a conventional microscope slide after aerosolization by blowing air into a tube of pollen. Figure 2a shows pollen grains illuminated with red laser light and imaged as a standard micrograph, with the camera arm ($\theta$) at 0°. Figure 2b is taken with illumination by the red and violet lasers simultaneously (wavelengths 650 and 405 nm, respectively). Dots on the left and right of each streak correspond to monochromatic images of the particles illuminated by the red and violet lasers, respectively. These appear as washed-out dots devoid of much color and large in size, as a result of the intensity of the illuminating lasers which saturate the detector. The swaths of color between the dots are due to fluorescence induced from the pollen particles. It should be noted that each of the spectral streaks in Fig. 2b–d can be related to specific particles by way of their images in Fig. 2a. Figure 2c shows an example white-light scattering spectra after polychromatic illumination by a tungsten filament. Figure 2d shows an identical image to that of Fig. 2b but without the red laser and with the blocking filter in place. In this way, the fluorescence spectra can be detected more sensitively, without washout from the red and violet lasers. By comparing Fig. 2c and d, one can see that the relative fraction of pollen particles fluorescent in this sample is nearly 100 %, since this particulate sample is made up of a single kind of relatively highly fluorescent particles. A particle-by-particle comparison is somewhat more difficult,

because each spectral swath (Fig. 2b–d) extends to the left from the non-dispersed particle location (Fig. 2a), which in some cases causes the swaths of multiple particles to overlap and in other cases causes the spectrum to be dispersed to a point out of the field of view. A more detailed analysis of all individual particles in Fig. 2 is described in the Supplement (Fig. S1).

Two laser spots of known wavelength give the ability to calibrate the pixel location with respect to wavelength for each of the spectral swaths. The wavelength scale for each particle is established by determining the wavelength dispersion from the positions in pixel numbers of the red and violet calibration spots, assuming a linear dependence of wavelength on distance in the plane of focus. Making use of the open-source program suite Image J (Rasband, 1997), one draws a box in the region of interest closely around the spectral swath. Employing the program's ability to determine average intensity at each horizontal pixel location on the swath, the data are presented in two columns – one column corresponding to horizontal pixel number and the other column corresponding to average light intensity detected at the given pixel number. These data columns are entered into a spreadsheet, and the pixel numbers are converted to a column of wavelength values using the dispersion calibration already determined.

Figure 3 shows the normalized fluorescence spectrum of three particles from the fluorescence image in Fig. 2d acquired by determining the intensity as a function of wavelength, as discussed above. The result is a wide peak centered at ca. 500 nm, broadly consistent with previous literature for many types of pollen (Hill et al., 2009; Pan et al., 2011; Pöhlker et al., 2013, 2012). A secondary peak, caused by the color camera pixels centered at ca. 600 nm, is also clear and will be discussed in a following section.

### 2.3 Some practical considerations

As a practical matter, the density of particles distributed on the slide should be sufficiently sparse that the spectral swaths do not overlap if individual particle spectra are to be determined. This requirement arises as a result of the fact that the entire field of view is illuminated at once, ideally exciting many, e.g., 5–30, particles. The wider the spectral range desired, the more this effect is enhanced. This particle density limitation is diminished, however, if one is interested primarily in the relative fraction of particles that fluoresce at a given excitation wavelength.

The technique introduced here also presents fundamental limitations in spectral resolution, influenced, in part, by particle size and homogeneity. For example, fluorescence emitted from the near side of a large particle at a given wavelength and $\theta$ angle will be dispersed at the same $\theta$ angle to a dissimilar point in the color swath from the far side of the same particle. This will blur the fluorescence spectrum in wavelength space increasingly as a function of particle size. Additionally, if a given particle is inhomogeneous in composition, the fluorescence spectrum emitted by two points on the particle will be dissimilar, and thus the resultant spectrum will appear somewhat smeared. Fluorescence emission bands are fundamentally broad and smooth, however, and so the extent of the associated smearing due to particle size or inhomogeneity does not practically impact the observed spectra for particles that are smaller than many tens of microns.

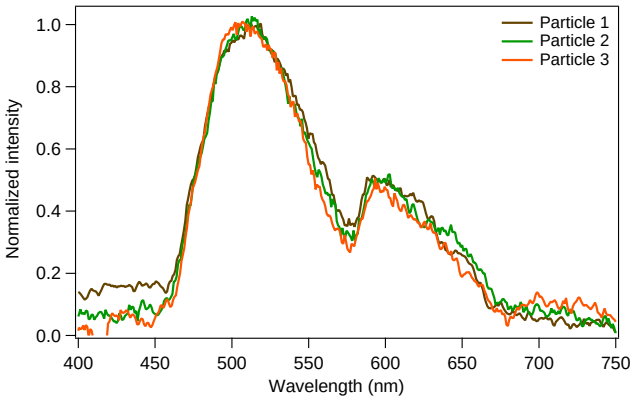


**Figure 3.** Fluorescence spectra of three individual paper mulberry pollen particles (*Broussonetia payrifera*) illuminated by 405 nm diode laser (Fig. 2d). Emission wavelength was calibrated using 405 and 650 nm laser points (Fig. 2b). All spectra were normalized to 1.0 maximum peak height.

## 3 Applications

In Fig. 4 we present images for two different collections of particles that highlight the simplest application of the instrument, which is to estimate the fraction of particles in a mixture that exhibit fluorescence. This can be achieved irrespective of whether emission spectra are analyzed and can have important application to a number of scientific questions. For example, the UV-APS has been frequently applied to the detection of bioaerosols in ambient air (Huffman et al., 2010), but it cannot provide spectrally resolved information and thus essentially provides information only about the fraction of particles that exhibit fluorescence at a given set of excitation and emission wavelengths. Figure 4 shows images associated with particulate samples of polydisperse particle size, as opposed to those shown in Fig. 2 which are very uniform in size.

### 3.1 Outdoor sample particles

The particles shown in Fig. 4a–c (top panel) were collected by leaving a glass microscope slide lying horizontally on a table 3 ft above ground level outdoors in Tucson, Arizona, for 24 h in the wintertime in clear weather. The comparison of the fluorescence image (Fig. 4c) with the elastic scattering image (Fig. 4b) is an illustration that the fraction of

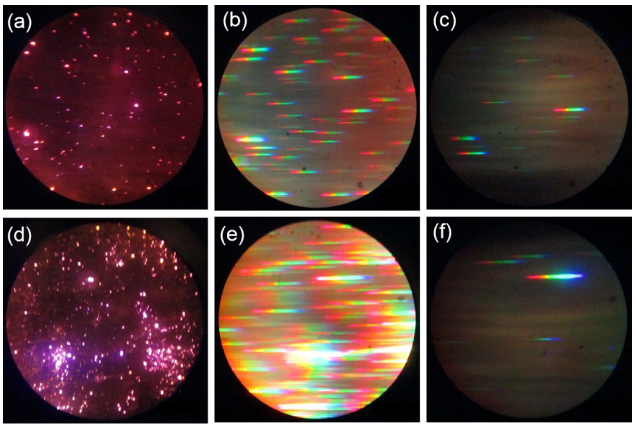


**Figure 4.** Images showing minority of fluorescent particles amidst large quantity of other particles. Top panels **(a–c)**: outdoor ambient particles collected via natural settling onto microscope slide. Bottom panels **(d–f)**: ground optical fused quartz particles. First column **(a, d)** shows conventional micrograph images ($\theta = 0$) illuminated with red laser light. Second column **(b, e)** shows white-light scattering spectra after illumination of same scene with polychromatic light from tungsten source. Third column **(c, f)** shows fluorescence spectra after illumination of same scene with 405 nm diode laser and blocking filter in place. Images acquired magnified using 10× objective.

aerosol particles exhibiting fluorescence is relatively easily determined without needing to analyze spectra and thus with little image processing. In fact, a rough idea about the relative fluorescent fraction can be achieved by eye simply by looking at camera images using both illumination schemes (e.g., Fig. 4b–c). The count for elastic scattering particles, which should comprise all particles both fluorescent and non-fluorescent, is ca. 46 in this example, whereas the number count of the brightly fluorescent particles is ca. 7. Thus the fraction of total particles that are fluorescent, and presumably of biological origin, is 7/46 here, or ca. 9 %, which is broadly consistent with typical ambient measurements, though fluorescent biological aerosol concentrations and properties vary widely by season and geography (Huffman et al., 2013; Schumacher et al., 2013). This fraction is highly dependent on the threshold one applies to categorize a given particle as fluorescent or not. Observed fluorescence intensity is also strongly a function of several factors, including particle size, fluorophore amount and quantum yield, intensity of excitation source, instrument optics, and camera exposure time (e.g., Hill et al., 2001, 2013, 2015; Pöhlker et al., 2012; Sivaprakasam et al., 2011). Most fluorescence-based aerosol detectors are faced with the conceptual challenge of how best to define minimum detectable fluorescence, and the sensitivity of a given detector will significantly influence the comparison of the relative fraction of fluorescent particles detected by any two instruments or types of instruments (e.g., Healy et al., 2014; Hernandez et al., 2016; Huffman et al., 2012; Saari et al., 2013). As mentioned, the particle size contributes significantly to the detectability of fluorescence from individual particles. All particles chosen for discussion here are relatively large (e.g., > 10 µm) in order to highlight the overall technique and concepts. It should be noted, however, that the instrument is not fundamentally limited to such large particles and can be applied to particles of 1 µm in diameter, or smaller, if higher microscope magnification (e.g., 40×) is utilized and the parameters influencing observed fluorescence intensity are managed appropriately. We have acquired spectra of individual particles as small as 0.96 µm (e.g., Fig. S2), though this is not intended to be presented as a lower limit. Further limitations will be explored in follow-up studies.

### 3.2 Fused silica particles

For the purpose of illustrating results for a particle collection expected to show no fluorescence, we prepared a collection of particles by grinding a piece of optical fused silica with an agate mortar and pestle. The optical silica of the starting material shows no appreciable fluorescence in bulk throughout the visible spectral region. A large spread of particle sizes is apparent in the micrograph of Fig. 4d, with many overlapping elastic scattering spectra apparent under illumination by the white light of a tungsten lamp (Fig. 4e). Figure 4f, however, shows one unexpected, strongly fluorescent particle and approximately three to five other weakly fluorescent particles out of the 200–250 particles in the image (e.g., ∼ 2 %). The elastic scattering streaks (Fig. 4e) for these particles is not particularly remarkable. Our interpretation is that the very few fluorescent particles observed are contaminants of fluorescent material which entered into the mixture during grinding or handling in a relatively dirty laboratory and which had previously contained various pollen particles. We refer to the image series in Fig. 4d–f as "a fluorescent needle in an elastic scattering haystack". This example illustrates how fluorescent impurities might easily be detected at a glance with our apparatus even in the presence of a large majority of non-biological, or otherwise non-fluorescent, particles and without needing to go through the extra step to extract the actual spectra. Analyzing images in this way also removes the restriction of limiting spectral swaths from overlapping and enables a user to collect a rather large number of particles in one field of view (e.g., hundreds), compared to the far smaller number limiting the analysis if determination of individual spectra is desired. The collection and analysis of particles in this case can be very rapid and yet can provide a powerful diagnostic tool by positively identifying the approximate fraction of fluorescent impurities in a collection of particles.

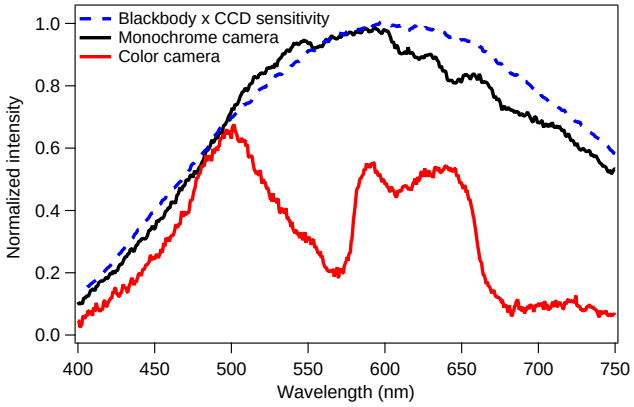


**Figure 5.** Comparison of white-light scattering from ground sodium chloride (NaCl) particle detected by color (solid red) and monochrome (solid black) cameras. Reference spectrum (dashed blue) shows calculated blackbody radiator at 3000 K multiplied by CCD sensitivity curve as an estimate of light intensity as a function of wavelength expected at detector. Red curve was normalized to 1.0 and then scaled down by an arbitrary value to show reduced emission intensity above 500 nm.

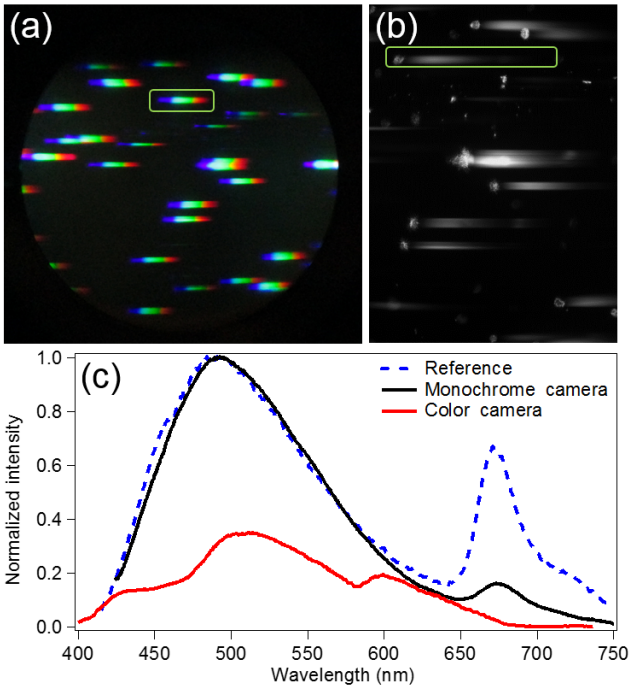


**Figure 6.** Spectral images and associated spectra for individual particles of Kentucky bluegrass (*Poa pratensis*) pollen. Both images show fluorescence of particles illuminated by 405 nm diode laser and utilizing 420 nm long-pass blocking filter. **(a)** Color camera detection. **(b)** Black-and-white camera detection. **(c)** Spectra of one particle from each image (boxed particle from **a, b** shown). Reference spectrum (dashed line) from microplate reader spectrofluorometer showing bulk average of ∼5 mg of material. Spectra from monochrome camera and reference technique normalized to peak height of 1.0. Spectrum from color camera arbitrarily scaled to show reduced intensity of collection compared to monochrome camera. Images acquired magnified using 10× objective.

## 4 Comparison of black-and-white with color cameras

Results presented to this point have been based on images taken using a Canon Powershot A2300 HD color camera, which is a simple point-and-shoot digital camera costing less than USD 100. It was chosen to promote the goal of producing a relatively low-cost apparatus. We have also used a more sophisticated b/w or monochrome camera – a Lumenara Infinity 2-1R, costing about USD 2000. Color cameras in general have several disadvantages compared to b/w cameras, as well as some advantages. They use CCD or CMOS detector arrays with three different color pixels and filters having peak sensitivities in (for example) the red, green, and blue. When a broad continuum of light is incident on such a detector, as from a tungsten lamp or a broadband fluorescence spectrum from a pollen grain, the otherwise smooth spectral curve will show variations due to the color-pixel characteristics. Figure 5 shows this effect experimentally with the white-light spectrum from an incandescent tungsten filament bulb (General Electric, Miniature Lamp 210, B6, 6.5 V) scattered from ground particles of sodium chloride (NaCl; Sigma Aldrich, CAS no. 7647-14-5) and independently detected by the monochrome camera and color camera discussed above. Each NaCl particle is expected to exhibit reasonably smooth scattering vs. wavelength, because its large size relative to the wavelength and its irregular shape do not promote the various sphere-like resonances expected from Mie theory (Bohren and Huffman, 1983). The monochrome camera yields a relatively smooth, broad scattering curve. For comparison, Fig. 5 also shows the emission spectrum from a 3000 Kelvin blackbody, as an approximation of the emission from the heated tungsten filament source used for white light, multiplied by the theoretical sensitivity curve of the CCD used in the monochrome camera[1]. The theoretical curve represents the spectrum that the CCD should detect assuming the particle does not introduce any wavelength-dependent scattering features. In this case the measured elastic scattering curve (black line) matches closely with the theoretical curve (blue, dashed line), suggesting that the monochrome camera introduces very little aberration as a function of wavelength. In contrast, the color camera shows a spectrum with pronounced peaks that are introduced by the different color pixels. These strong variations in the spectra from color cameras are difficult to correct for and are not present in monochrome cameras. Another disadvantage of most color cameras is the incorporation of an infrared blocking filter which is added to exclude light of wavelengths longer than deep red in order to produce a more natural color in the image but which limits

[1]http://www.opticstar-ccd.com/Images/Astronomy/Imagers/OS/Common/QE-ICX205AL-594x255.jpg

the red spectral range of fluorescence and elastic scattering detection.

To further illustrate both of these undesirable features of color cameras, Fig. 6 shows a comparison of images from particles of Kentucky bluegrass pollen (*Poa pratensis*, also known as smooth or common meadow grass; 20–120 µm; Allergon SKU 0116), recorded and analyzed as described above to derive the spectral curves from both the b/w (black curve) and the color camera (red curve). The b/w camera results show a broad fluorescence band peaking near 490 nm and a somewhat narrower band near 680 nm. The latter band is assigned to chlorophyll *a*, which is present in most grass pollens (Maxwell and Johnson, 2000; O'Connor et al., 2011, 2014). A reference spectrum of bulk bluegrass pollen powder was achieved by adding ca. 5 mg of pollen to one well of a black 96-well plate (Fisher Scientific, 07-200-329) and recording a fluorescence emission spectrum at 405 nm excitation using a microplate reader spectrofluorometer (Infinite M1000 Pro, Tecan, Männerdorf, Switzerland). This technique cannot provide single-particle spectra, as discussed previously, but delivers a spectrum as an average of the bulk powder. The peak locations in the reference and b/w camera spectra are identical, though the relative ratio of chlorophyll peak to main peak is higher in the reference spectrum. This is expected, as individual pollen grains exhibit markedly different concentrations of chlorophyll as a result of differences in age and physiological state (Boyain-Goitia et al., 2003; Pöhlker et al., 2013). The color camera also shows a band near 490 nm as well as an irregular and asymmetric peak near 600 nm, with no sign of the chlorophyll band. The ∼ 600 nm structure appears in the color camera image due to the color-pixel effect discussed above. The absence of the chlorophyll peak from the color camera is likely due to the presence of the infrared blocking filter in the color camera only, which removes the transmission of chlorophyll transmission.

Notwithstanding the disadvantages of the color camera, it has several pleasant and useful features. First of all, the images of the spectra are simply interesting and beautiful! This may even be a non-trivial benefit when soliciting effort from citizen scientists, because the images can produce captivating, artistic views of the natural, microscopic world. From a practical scientific viewpoint, the colors are valuable for quickly getting oriented to the approximate wavelength positions of spectral features, which may be evident in the spectral swaths even without further processing. Also, the spectral colors are very useful when higher-order spectra ($n > 1$ in Eq. 1) are present, which may result in overlapping orders. These can be easily sorted out if colored swaths are present, while they can become confusing when viewing the colorless black and gray images from a monochrome camera. For many investigations we have utilized both cameras in tandem, and perhaps the best solution in the future will be to use a combination of a b/w camera along with a color camera for standard usage. The two could be arranged on optical axes at 90° from one another with a "flip mirror" used as a quick method to switch from one to the other.

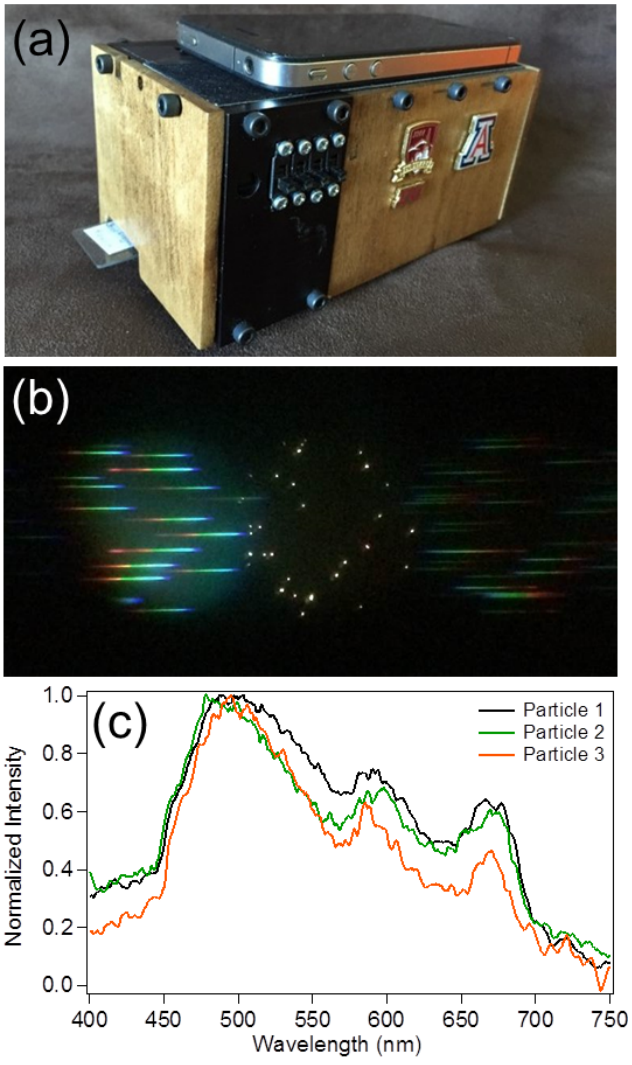


**Figure 7.** Smartphone spectrofluorometer prototype. **(a)** Photograph of iPhone spectrometer. **(b)** Standard micrograph (dots in center) and fluorescence swaths (on left and right) collected as single image with iPhone 5s shown in panel **(a)** using 10× objective. Particles are Kentucky bluegrass pollen (*Poa pratensis*). **(c)** Spectra of three of the particles from panel **(b)**, normalized to peak height of 1.0. As shown, field of view is a 2 mm circle. Approximate distance from objective lens to camera is 6 cm.

## 5 Smartphone embodiment

Because of the development of smartphones for the global consumer market, smartphones now contain highly sophisticated cameras built into the devices which are lightweight, low in electrical power, and relatively inexpensive. These devices also can have other useful capabilities such as GPS sensors providing geographic location, temperature and time de-

tection, and the capability of connecting easily to the Internet for almost immediate sharing of data. We built and tested two prototypes of the particle spectrometer – one for an iPhone and one for an Android phone. Figure 7a shows a photograph of the iPhone version, with an iPhone model 5s (Apple, Inc.) placed on top. The iPhone uses its own battery for the camera and other smartphone functions. Behind the wooden panels of the instrument body ($13.3 \times 13.3 \times 7.4$ cm; 58 g) are the same optical components discussed above regarding the benchtop version. There is an objective lens, blocking filter, and diffraction grating as well as three light sources (red and violet laser diodes and tungsten light source) operated by two AA batteries. The microscope slide onto which particles are collected can be slipped through a hole in the exterior casing, and four switches on the side of the instrument, attached to the anodized aluminum panel, operate the light sources so that images can be acquired without opening the case to ambient light. At present the little instrument only acquires and saves images, which must be downloaded to a computer for processing, as described earlier in this paper. A future goal is to utilize a combination of onboard and cloud-based image processing to provide spectra to the smartphone user.

The second panel (Fig. 7b) shows a typical image of Kentucky bluegrass pollen taken with this instrument. The image shows fluorescence streaks from individual particles, similar to images acquired using the benchtop instrument (Fig. 2) as discussed above. Because of the wide angle of acceptance of the iPhone camera, the $\theta = 0$ microscope image is visible in the middle of the image as well as first-order diffraction streaks to both the left and right. The fluorescence intensity of the right-most image is less than for the light diffracted to the left due to the blaze angle of the grating. The peak at $\sim 600$ nm arises from the wavelength dependence of the color pixels, as discussed above. It is important to note here, however, that the peak at $\sim 680$ nm shows the chlorophyll *a* peak, in contrast to the absence of this peak when using the Canon color camera discussed previously.

## 6 A vision for broad-scale use

Our vision for broad-scale use of a portable version of the instruments is twofold. First, the ability to sample and analyze fluorescence spectra of airborne particles has been limited because UV-LIF instruments are so expensive that they are typically deployed one at a time in a given region. This means that only in rare cases have such instruments been utilized to record information about bioaerosols to understand spatial variability. With the development of a sampler for particle collection hyphenated to the optical analysis tool described above, it could be possible for many units to be constructed inexpensively and deployed simultaneously, thus allowing for the collection and analysis of particles in a network across a chosen area. For this to become a reality we are working towards a future model which will incorporate automatic sampling and analysis capabilities, for example utilizing a Raspberry Pi camera (Raspberry Pi Foundation, United Kingdom) to remove the need for a dedicated smartphone for each unit.

A second vision, specifically applicable to the smartphone version, is to involve interested citizen scientists from around the world who already possess the most expensive component of this fluorescent instrument – the smartphone. Our opto-mechanical additions to the smartphone meet the desired requirements of being relatively lightweight, low power and inexpensive. At an estimated cost in bulk of about USD 200, some 500 units (not counting the smartphone) could perhaps be produced for the approximately USD 100 000 price of a real-time commercial sensor such as the WIBS. Interested persons could be enlisted to collect and measure particles and send the results back to a central computer where analysis would be done. Some simplified results, such as the percentage of fluorescent particles of biological origin, might be returned to the volunteer measurer to stimulate and maintain their interest. Or a cloud-computer may allow spectra from individual particles to be clustered and compared with a database of spectral standards for course-level discrimination (Pan et al., 2012; Pinnick et al., 2013; Robinson et al., 2013). Citizen-scientist-assisted collection of data about fluorescent aerosol particles using this technique could help change the face of this area of science by acquiring orders of magnitude more data points in time and space than are currently available.

Although this paper has emphasized the applications of the instrument for acquiring spectral fluorescence of particles, there may occur even more applications for elastic scattering from particles, which can be obtained using white-light illumination as in Fig. 2c rather than 2d. The technique of acquiring spectra from individual particles could perhaps also be applied to the acquisition of Raman scattering spectra, though this would introduce additional technical challenges such as the need for relatively high spectral resolution, which is compromised in our slitless spectrometer technique. Recently an instrument for real-time detection of single particles in air by Raman spectroscopy has been made commercially available (Doughty and Hill, 2016; Ronningen et al., 2014). The instrument described here could be developed in the future to provide Raman spectra of individual atmospheric particles at significantly reduced cost compared to existing Raman microscopes, albeit with reduced spectral resolution and signal-to-noise ratio.

## 7 Summary and conclusions

We have described the development of a small, lightweight, and low-cost instrument which uses the principle of a slitless spectrograph to determine both the elastic scattering spectra and inelastic spectra (such as fluorescence) for each particle in a many-particle collection on a glass microscope slide

or other surface. In addition to a benchtop model composed of standard microscope parts, we have shown a small instrument as an attachment to a smartphone or other small digital camera producing data in the form of images that can be sent immediately from almost any location on the earth to a remote master computer for analysis. In the case of its primary intended use, the instrument can provide separate spectral images of fluorescence and elastic scatter which allow direct determination of the ratio of biological particles to total particles. At present there are no inexpensive, autonomous sensors available that can estimate the concentration of mold spores or pollen types that can exacerbate human allergies. The portable version of the instrument may provide a critical leap in the detection of several types of biological aerosol particles. For example, by differentiating between chlorophyll-containing pollen and other pollen types, the detector could provide a quick quantification of grass-type pollens (i.e., *Dactylis glomerata*, or orchard grass) that are responsible for many cases of hay fever and allergenic rhinitis across the world (D'Amato et al., 2007; O'Connor et al., 2014).

The strong benefits of the described technique include that many particles can be analyzed simultaneously and that fluorescence spectra can be rapidly acquired for individual particles, each at multiple wavelengths, and at a cost potentially orders of magnitude lower than existing techniques. Further, the technique provides the possibility to probe at a glance for contamination of fluorescent particles that could contaminate a collection of non-fluorescent material, even without needing to analyze spectra.

## 8 Data availability

Spectral data are available upon request.

**The Supplement related to this article is available online at doi:10.5194/amt-9-3987-2016-supplement.**

*Acknowledgements.* The authors acknowledge Brason Holt for assistance with laboratory experiments. Donald R. Huffman acknowledges the $C_{60}$ Patent Royalty Fund of the University of Arizona for support. J. Alex Huffman and Benjamin E. Swanson acknowledge funding from the University of Denver Professional Research Opportunities for Faculty (PROF) program.

Edited by: J. Schneider
Reviewed by: two anonymous referees

## References

Abell, G. O.: Exploration of the Universe, Holt, Rinehart & Winston of Canada Ltd., 1969.

Bohren, C. F. and Huffman, D. R.: Absorption and Scattering of Light By Small Particles, John Wiley & Sons, New York, NY, 1983.

Boyain-Goitia, A. R., Beddows, D. C. S., Griffiths, B. C., and Telle, H. H.: Single-pollen analysis by laser-induced breakdown spectroscopy and Raman microscopy, Appl. Opt., 42, 6119–6132, 2003.

Cheng, J., Liu, Y., Cheng, X., He, Y., and Yeung, E. S.: Real Time Observation of Chemical Reactions of Individual Metal Nanoparticles with High-Throughput Single Molecule Spectral Microscopy, Anal. Chem., 82, 8744–8749, 2010.

D'Amato, G., Cecchi, L., Bonini, S., Nunes, C., Annesi-Maesano, I., Behrendt, H., Liccardi, G., Popov, T., and van Cauwenberge, P.: Allergenic pollen and pollen allergy in Europe, Allergy, 62, 976–990, 2007.

Després, V. R., Huffman, J. A., Burrows, S. M., Hoose, C., Safatov, A. S., Buryak, G. A., Fröhlich-Nowoisky, J., Elbert, W., Andreae, M. O., Pöschl, U., and Jaenicke, R.: Primary Biological Aerosol Particles in the Atmosphere: A Review, Tellus B, 64, 15598, doi:10.3402/tellusb.v64i0.15598, 2012.

Doughty, D. C. and Hill, S. C.: Automated aerosol Raman spectrometer for semi-continuous sampling of atmospheric aerosol, J. Quant. Spectrosc. Ra., doi:10.1016/j.jqsrt.2016.06.042, online first, 2016.

Douwes, J., Thorne, P., Pearce, N., and Heederik, D.: Bioaerosol health effects and exposure assessment: Progress and prospects, Ann. Occup. Hyg., 47, 187–200, 2003.

Foot, V. E., Kaye, P. H., Stanley, W. R., Barrington, S. J., Gallagher, M., and Gabey, A.: Low-cost real-time multi-parameter bio-aerosol sensors, Proc. SPIE 7116, Optically Based Biological and Chemical Detection for Defence IV, 71160I, doi:10.1117/12.800226, 2008.

Fröhlich-Nowoisky, J., Kampf, C. J., Weber, B., Huffman, J. A., Pöhlker, C., Andreae, M. O., Lang-Yona, N., Burrows, S. M., Gunthe, S. S., Elbert, W., Su, H., Hoor, P., Thines, E., Hoffmann, T., Després, V. R., and Pöschl, U.: Bioaerosols in the Earth System: Climate, Health, and Ecosystem Interactions, Atmos. Res., doi:10.1016/j.atmosres.2016.07.018, online first, 2016.

Gabey, A. M., Gallagher, M. W., Whitehead, J., Dorsey, J. R., Kaye, P. H., and Stanley, W. R.: Measurements and comparison of primary biological aerosol above and below a tropical forest canopy using a dual channel fluorescence spectrometer, Atmos. Chem. Phys., 10, 4453–4466, doi:10.5194/acp-10-4453-2010, 2010.

Hairston, P. P., Ho, J., and Quant, F. R.: Design of an instrument for real-time detection of bioaerosols using simultaneous measurement of particle aerodynamic size and intrinsic fluorescence, J. Aerosol Sci., 28, 471–482, 1997.

Hale, G. E. and Wadsworth, F. L. O.: The Modern Spectroscope: XIX. The Objective Spectroscope, Astrophys. J., 4, p. 54, doi:10.1086/140241, 1896.

Healy, D. A., Huffman, J. A., O'Connor, D. J., Pöhlker, C., Pöschl, U., and Sodeau, J. R.: Ambient measurements of biological aerosol particles near Killarney, Ireland: a comparison between real-time fluorescence and microscopy techniques, Atmos. Chem. Phys., 14, 8055–8069, doi:10.5194/acp-14-8055-2014, 2014.

Hernandez, M., Perring, A. E., McCabe, K., Kok, G., Granger, G., and Baumgardner, D.: Chamber catalogues of optical and fluorescent signatures distinguish bioaerosol classes, Atmos. Meas. Tech., 9, 3283–3292, doi:10.5194/amt-9-3283-2016, 2016.

Hill, S. C., Pinnick, R. G., Niles, S., Fell, N. F., Pan, Y. L., Bottiger, J., Bronk, B. V., Holler, S., and Chang, R. K.: Fluorescence from airborne microparticles: dependence on size, concentration of fluorophores, and illumination intensity, Appl. Opt., 40, 3005–3013, 2001.

Hill, S. C., Mayo, M. W., and Chang, R. K.: Fluorescence of Bacteria, Pollens, and Naturally Occurring Airborne Particles: Excitation/Emission Spectra, Army Research Laboratory, Adelphi, MD, 2009.

Hill, S. C., Pan, Y. L., Williamson, C., Santarpia, J. L., and Hill, H. H.: Fluorescence of bioaerosols: mathematical model including primary fluorescing and absorbing molecules in bacteria, Opt. Express, 21, 22285–22313, 2013.

Hill, S. C., Williamson, C. C., Doughty, D. C., Pan, Y. L., Santarpia, J. L., and Hill, H. H.: Size-dependent fluorescence of bioaerosols: Mathematical model using fluorescing and absorbing molecules in bacteria, J. Quant. Spectrosc. Ra., 157, 54–70, 2015.

Huffman, J. A., Treutlein, B., and Pöschl, U.: Fluorescent biological aerosol particle concentrations and size distributions measured with an Ultraviolet Aerodynamic Particle Sizer (UV-APS) in Central Europe, Atmos. Chem. Phys., 10, 3215–3233, doi:10.5194/acp-10-3215-2010, 2010.

Huffman, J. A., Sinha, B., Garland, R. M., Snee-Pollmann, A., Gunthe, S. S., Artaxo, P., Martin, S. T., Andreae, M. O., and Pöschl, U.: Size distributions and temporal variations of biological aerosol particles in the Amazon rainforest characterized by microscopy and real-time UV-APS fluorescence techniques during AMAZE-08, Atmos. Chem. Phys., 12, 11997–12019, doi:10.5194/acp-12-11997-2012, 2012.

Huffman, J. A., Prenni, A. J., DeMott, P. J., Pöhlker, C., Mason, R. H., Robinson, N. H., Fröhlich-Nowoisky, J., Tobo, Y., Després, V. R., Garcia, E., Gochis, D. J., Harris, E., Müller-Germann, I., Ruzene, C., Schmer, B., Sinha, B., Day, D. A., Andreae, M. O., Jimenez, J. L., Gallagher, M., Kreidenweis, S. M., Bertram, A. K., and Pöschl, U.: High concentrations of biological aerosol particles and ice nuclei during and after rain, Atmos. Chem. Phys., 13, 6151–6164, doi:10.5194/acp-13-6151-2013, 2013.

Jenkins, F. A. and White, H. E.: Fundamentals of optics, McGraw-Hill Education, 1957.

Kaye, P. H., Stanley, W. R., Hirst, E., Foot, E. V., Baxter, K. L., and Barrington, S. J.: Single particle multichannel bio-aerosol fluorescence sensor, Opt. Express, 13, 3583–3593, 2005.

Kiselev, D., Bonacina, L., and Wolf, J.-P.: Individual bioaerosol particle discrimination by multi-photon excited fluorescence, Opt. Express, 19, 24516–24521, 2011.

Lakowicz, J. R.: Principles of Fluorescence Specrtroscopy, Springer US, 954 pp., 2010.

Manninen, A., Putkiranta, M., Rostedt, A., Saarela, J., Laurila, T., Marjamaki, M., Keskinen, J., and Hernberg, R.: Instrumentation for measuring fluorescence cross sections from airborne micro-sized particles, Appl. Opt., 47, 110–115, 2008.

Maxwell, K. and Johnson, G. N.: Chlorophyll fluorescence – a practical guide, J. Exp. Bot., 51, 659–668, 2000.

Möhler, O., DeMott, P. J., Vali, G., and Levin, Z.: Microbiology and atmospheric processes: the role of biological particles in cloud physics, Biogeosciences, 4, 1059–1071, doi:10.5194/bg-4-1059-2007, 2007.

Morris, C. E., Conen, F., Huffman, J. A., Phillips, V., Pöschl, U., and Sands, D. C.: Bioprecipitation: a feedback cycle linking Earth history, ecosystem dynamics and land use through biological ice nucleators in the atmosphere, Glob. Change Biol., 20, 341–351, 2014.

O'Connor, D. J., Iacopino, D., Healy, D. A., O'Sullivan, D., and Sodeau, J. R.: The intrinsic fluorescence spectra of selected pollen and fungal spores, Atmos. Environ., 45, 6451–6458, 2011.

O'Connor, D. J., Lovera, P., Iacopino, D., O'Riordan, A., Healy, D. A., and Sodeau, J. R.: Using spectral analysis and fluorescence lifetimes to discriminate between grass and tree pollen for aerobiological applications, Anal. Method., 6, 1633–1639, 2014.

Pan, Y. L., Hartings, J., Pinnick, R. G., Hill, S. C., Halverson, J., and Chang, R. K.: Single-particle fluorescence spectrometer for ambient aerosols, Aerosol Sci. Technol., 37, 628–639, 2003.

Pan, Y. L., Hill, S. C., Pinnick, R. G., Huang, H., Bottiger, J. R., and Chang, R. K.: Fluorescence spectra of atmospheric aerosol particles measured using one or two excitation wavelengths: Comparison of classification schemes employing different emission and scattering results, Opt. Express, 18, 12436–12457, 2010.

Pan, Y.-L., Hill, S. C., Pinnick, R. G., House, J. M., Flagan, R. C., and Chang, R. K.: Dual-excitation-wavelength fluorescence spectra and elastic scattering for differentiation of single airborne pollen and fungal particles, Atmos. Environ., 45, 1555–1563, 2011.

Pan, Y.-L., Huang, H., and Chang, R. K.: Clustered and integrated fluorescence spectra from single atmospheric aerosol particles excited by a 263-and 351-nm laser at New Haven, CT, and Adelphi, MD, J. Quant. Spectrosc. Ra., 113, 2213–2221, 2012.

Perring, A. E., Schwarz, J. P., Baumgardner, D., Hernandez, M. T., Spracklen, D. V., Heald, C. L., Gao, R. S., Kok, G., McMeeking, G. R., McQuaid, J. B., and Fahey, D. W.: Airborne observations of regional variation in fluorescent aerosol across the United States, J. Geophys. Res.-Atmos., 120, 1153–1170, 2015.

Pinnick, R. G., Fernandez, E., Rosen, J. M., Hill, S. C., Wang, Y., and Pan, Y. L.: Fluorescence spectra and elastic scattering characteristics of atmospheric aerosol in Las Cruces, New Mexico, USA: Variability of concentrations and possible constituents and sources of particles in various spectral clusters, Atmos. Environ., 65, 195–204, 2013.

Pöhlker, C., Huffman, J. A., and Pöschl, U.: Autofluorescence of atmospheric bioaerosols – fluorescent biomolecules and potential interferences, Atmos. Meas. Tech., 5, 37–71, doi:10.5194/amt-5-37-2012, 2012.

Pöhlker, C., Huffman, J. A., Förster, J.-D., and Pöschl, U.: Autofluorescence of atmospheric bioaerosols: spectral fingerprints and taxonomic trends of pollen, Atmos. Meas. Tech., 6, 3369–3392, doi:10.5194/amt-6-3369-2013, 2013.

Pöschl, U. and Shiraiwa, M.: Multiphase Chemistry at the Atmosphere–Biosphere Interface Influencing Climate and Public Health in the Anthropocene, Chem. Rev., 115, 4440–4475, 2015.

Pöschl, U., Martin, S. T., Sinha, B., Chen, Q., Gunthe, S. S., Huffman, J. A., Borrmann, S., Farmer, D. K., Garland, R. M., Helas, G., Jimeney, J. L., King, S. M., Manzi, A., Mikhailov, E., Pauliquevis, T., Petters, M. D., Prenni, A. J., Roldin, P., Rose, D., Schneider, J., Su, H., Zorn, S. R., Artaxo, P., and Andreae,

M. O.: Rainforest Aerosols as Biogenic Nuclei of Clouds and Precipitation in the Amazon, Science, 329, 1513–1516, 2010.

Rasband, W. S.: ImageJ, US National Institutes of Health, Bethesda, Maryland, USA, http://imagej.nih.gov/ij/, 1997–2016.

Robinson, N. H., Allan, J. D., Huffman, J. A., Kaye, P. H., Foot, V. E., and Gallagher, M.: Cluster analysis of WIBS single-particle bioaerosol data, Atmos. Meas. Tech., 6, 337–347, doi:10.5194/amt-6-337-2013, 2013.

Ronningen, T., Schuetter, J., Wightman, J., and Murdock, A.: Raman spectroscopy for biological identification, in: Biological Identification: DNA Amplification and Sequencing, Optical Sensing, Lab-On-chip and Portable Systems, 313–333, 2014.

Saari, S., Reponen, T., and Keskinen, J.: Performance of Two Fluorescence-Based Real-Time Bioaerosol Detectors: BioScout vs. UVAPS, Aerosol Sci. Technol., 48, 371–378, 2013.

Saari, S., Reponen, T., and Keskinen, J.: Performance of Two Fluorescence-Based Real-Time Bioaerosol Detectors: BioScout vs. UVAPS, Aerosol Sci. Tech., 48, 371–378, 2014.

Schumacher, C. J., Pöhlker, C., Aalto, P., Hiltunen, V., Petäjä, T., Kulmala, M., Pöschl, U., and Huffman, J. A.: Seasonal cycles of fluorescent biological aerosol particles in boreal and semi-arid forests of Finland and Colorado, Atmos. Chem. Phys., 13, 11987–12001, doi:10.5194/acp-13-11987-2013, 2013.

Sivaprakasam, V., Huston, A. L., Scotto, C., and Eversole, J. D.: Multiple UV wavelength excitation and fluorescence of bioaerosols, Opt. Express, 12, 4457–4466, 2004.

Sivaprakasam, V., Pletcher, T., Tucker, J. E., Huston, A. L., McGinn, J., Keller, D., and Eversole, J. D.: Classification and selective collection of individual aerosol particles using laser-induced fluorescence, Appl. Opt., 48, B126–B136, 2009.

Sivaprakasam, V., Lin, H.-B., Huston, A. L., and Eversole, J. D.: Spectral characterization of biological aerosol particles using two-wavelength excited laser-induced fluorescence and elastic scattering measurements, Opt. Express, 19, 6191–6208, 2011.

Sodeau, J. R. and O'Connor, D. J.: Bioaerosol Monitoring of the Atmosphere for Occupational and Environmental Purposes, Compr. Anal. Chem., 73, 391–420, doi:10.1016/bs.coac.2016.02.012, 2016.

Xiong, B., Zhou, R., Hao, J., Jia, Y., He, Y., and Yeung, E. S.: Highly sensitive sulphide mapping in live cells by kinetic spectral analysis of single Au-Ag core-shell nanoparticles, Nat. Commun., 4, 1708, doi:10.1038/ncomms2722, 2013.